https://doi.org/10.5194/acp-2020-1007
Preprint. Discussion started: 28 October 2020

Atmospheric Chemistry and Physics Discussions

Sea waves impact on turbulent heat fluxes in the Barents Sea according to numerical modeling

Stanislav Myslenkov[1,2,3] Anna Shestakova[4], Dmitry Chechin[4,5]

[1]Lomonosov Moscow State University, 119991, Moscow, Russia

[2]Shirshov Institute of Oceanology RAS, 117997, Moscow, Russia

[3]Hydrometeorological Research Centre of the Russian Federation, 123242, Moscow, Russia

[4]A.M.Obukhov Institute of Atmospheric Physics RAS, 119017, Moscow, Russia

[5]Moscow Institute of Physics and Technology, 119017, Moscow, Russia

Correspondence to: Stanislav Myslenkov (stasocean@gmail.com)

Abstract. This paper investigates the impact of sea waves on turbulent heat fluxes in the Barents Sea. The COARE algorithm, meteorological data from reanalysis and wave data from the WW3 wave model results were used. The turbulent heat fluxes were calculated using the modified Charnock parameterization for the roughness length and several parameterizations, which explicitly account for the sea waves parameters. A catalog of storm wave events and a catalog of extreme cold-air outbreaks over the Barents Sea were created and used to calculate heat fluxes during extreme events.

The important role of cold-air outbreaks in the energy exchange of the Barents Sea and the atmosphere is demonstrated. A high correlation was found between the number of cold-air outbreaks days and turbulent fluxes of sensible and latent heat, as well as with the net flux of long-wave radiation averaged over the ice-free surface of the Barents Sea during a cold season.

The differences in the long-term mean values of heat fluxes calculated using different parameterizations for the roughness length are small and are on average 1-3% of the flux magnitude. Parameterizations of Taylor and Yelland and Oost et al. on average lead to an increase of the magnitude of the fluxes, and the parameterization of Drennan et al. leads to a decrease of the magnitude of the fluxes over the entire sea compared to the Charnock parameterization.

The magnitude of heat fluxes and their differences during the storm wave events exceed the mean values by a factor of 2. However, the effect of explicit accounting for the wave parameters is, on average, small and multidirectional, depending on the used parameterization for the roughness length. In the climatic aspect, it can be argued that the explicit accounting for sea waves in the calculations of heat fluxes can be neglected.

However, during the simultaneously observed storm waves and cold-air outbreaks, the sensitivity of the calculated values of fluxes to the used parameterizations increase along with the turbulent heat transfer increase. In some extreme cases, during storms and cold-air outbreaks, the difference reaches 700 W m^{-2}.

Keywords: Barents Sea; turbulent heat flux; Charnock parameter; COARE; wind wave hindcast; cold-air outbreaks

https://doi.org/10.5194/acp-2020-1007
Preprint. Discussion started: 28 October 2020

Atmospheric Chemistry and Physics Discussions

1. Introduction

Atlantic water undergoes a significant transformation in the Barents Sea where its characteristics, such as temperature, salinity and density, change. New water masses are formed which contain different volumes of the original Atlantic water (Ivanov and Timokhov, 2019). A significant part of the heat content of Atlantic water is spent on melting ice and heating the atmosphere influencing the climatic characteristics of the region (Rahmstorf and Ganopolski, 1999). To a large extent, the heat exchange between the Barents Sea and the atmosphere is carried out by the turbulent heat flux. The Barents Sea is known to be one of the most efficient heat sinks from the ocean to the atmosphere (Simonsen and Haugan, 1996). On average, turbulent heat transfer in the Barents Sea is about 30 W/m2, according to modeling data (Arthun and Schrum 2010). However, even rough reanalysis data show that in energy active zones near the ice edge, fluxes can reach 500 W/m2 (Hakkinen and Cavalieri 1989).The latter depends on the surface roughness, which is associated with the wind wave parameters. Thus, adequate representation of surface roughness is crucial for correct estimates of the surface heat flux.

The modern models of the atmosphere and ocean commonly use the Charnock formula (Charnock, 1955) as a parameterization of the aerodynamic roughness length over the water. The Charnock relationship represents a quadratic dependence of the roughness length on the friction velocity. The Charnock parameter as constant, which represents the proportionality coefficient between the roughness length and the square of friction velocity, used in the most frequently models and reanalyses (for example, in NCEP/NCAR, NCEP/CFSR, MERRA reanalyses). However, numerous studies of roughness behavior in different conditions according to observational data (e.g. Oost et al. 2002, Mahrt et al. 2003) showed that the Charnock parameter (coefficient) is not constant, especially in conditions of high wind speed and high waves. The Charnock formula is applicable when the wave state is in equilibrium with wind forcing, and does not take into account the age of the waves and such effects as wave breaking and spray formation.

Thereby, several parametrizations were proposed that explicitly or implicitly take into account the influence of such wave parameters as wave height, wave length and period on the sea surface roughness.

In the most simple modification of the Charnock formulation the Charnock parameter is set as a piecewise constant or a linear function of wind speed in order to fit the observations. In other parametrizations, the Charnock parameter explicitly depends on the wind wave parameters, usually the wave steepness (Taylor and Yelland 2001) and wave the age (Jones and Toba 2001, Oost et al. 2002, Drennan et al. 2003). More complex parameterizations are based on the relation between the roughness length and the wave momentum flux (Janssen 1991) and are typically used in coupled wave-atmosphere models, including ECMWF operational analysis and reanalyses (ECMWF 2007). Intercomparisons of different roughness parametrizations, including Taylor and Yelland (2001), Oost et al. (2002) and Drennan et al. (2003) parametrizations, did not reveal the best of them (Pan et al. 2008, Charles and Hemer 2013, Shimura et al. 2017, Kim et al. 2018, Prakash et al. 2019). Some studies have shown that Oost et al. parametrization overestimates the roughness of the sea surface in comparison with other schemes (Pan et al. 2008, Kim et al. 2018), and Drennan et al. parametrization usually gives a lower roughness (Charles and Hemer 2013).

The choice of roughness length parameterization affects primarily the momentum flux and turbulent heat transfer. The sensible and latent heat fluxes are calculated using also the roughness length for temperature and specific humidity, respectively. The ratio of the roughness lengths for scalars and momentum is typically parameterized as function of the Reynolds roughness number (Brutsaert 1982, Zilitinkevich et al. 2001, Renfrew et al. 2002, Brunke et al . 2011).

The turbulent heat transfer is parameterized using bulk formulae in most reanalyses, which differ in the choice of the parameterization for the roughness length for temperature and humidity, parameterization of the Charnock parameter, and of the universal functions describing the dependence of the transfer coefficients on the

https://doi.org/10.5194/acp-2020-1007
Preprint. Discussion started: 28 October 2020

Atmospheric Chemistry and Physics Discussions

surface layer stratification (Renfrew et al. 2002, Brunke et al. 2011). A list of the parameterizations used in the main reanalyses is given in the Appendix by Brunke et al. (2011).

The use of certain parameterization can significantly affect the value of the calculated heat and momentum fluxes. For instance, the difference in the total turbulent heat flux between the two most commonly used algorithms, NCAR (Large and Yeager, 2009) and COARE (Coupled Ocean Atmosphere Response Experiment) (Fairall et al. 1996), is 13 W/m^2 on average throughout the globe and reaches 15-20% of the flux magnitude in mid-latitudes and subpolar regions (Brodeau et al. 2017). Typical values of the average difference of turbulent fluxes produced by different algorithms and the observational data amount to 5-15 W/m^2. Unambiguously "the best set of parameterizations" of the roughness length and universal functions for calculating heat and momentum fluxes does not exist (Brunke et al. 2011;, Charles and Hemer 2013). Nevertheless, the widely used COARE algorithm (Fairall et al. 1996, Fairall et al. 2003), which is also embedded in satellite flux calculation algorithms, is considered the most reliable for calculating turbulent fluxes. Satellite products such as J-OFURO, HOAPS, and OAFlux (joint satellite and simulation product), use algorithms very similar to COARE (Brunke et al. 2011, Yu et al. 2011). The COARE algorithm offers a choice of Taylor and Yelland (2001) and Oost et al. (2002) roughness length parameterizations, which explicitly take into account the wind wave parameters.

Roughness length dependency on wind wave parameters is expected to have regional differences depending on the local features of the wave regime. According to studies of the wave climate of the Barents Sea (Wind and Wave…, 2003; Stopa et al., 2016; Liu Q. et al., 2016), a significant part of the year stormy weather prevails over the Barents Sea. The duration of periods in which the wind speed does not exceed 15 m/s in the winter months averages only 3–6 days. The mean wave height (probability of exceedance 50%) with a frequency of occurrence of 1 time per year is 6.1 m, and the maximum wave height (probability of exceedance 0.1%) is more than 19 m (Wind and Wave…, 2003). Such values indicate the high frequency of occurrence of extreme waves. The average significant wave heights of in the Barents Sea is 1.8–2.2 m for the central part of the Barents Sea (Myslenkov et al., 2019). The maximum of significant wave heights reaches 12–14 m in the central part of the Barents Sea. The storms with significant wave heights of more than 4 m are observed on average 70–80 times a year, with significant wave heights more than 5 m - 40–60 times a year. The interannual variability of the recurrence of storm waves is very large (for different years the number of cases can vary by a factor of 2–3) (Myslenkov et al., 2018, 2019).

Moreover, the wave climate of the Barents Sea is characterized by a significant influence of swell coming from the North Atlantic. Based on numerical experiments (Myslenkov et al., 2015), it was shown that the height of swell can reach 5 m with a period of 15-18 sec. The effect of swell is not taken into account in the Charnock relationship explicitly, which can cause errors in the calculated values of the roughness length and turbulent fluxes.

In addition to wind speed, the difference of temperature and specific humidity between the sea surface and air also affects the magnitude of turbulent heat fluxes over the sea. These differences reach particularly large values during the so-called cold-air outbreaks (CAOs). CAOs represent the advection of a dry and cold air mass onto the open sea originating from the Central Arctic or from the cold continents (Pithan et al., 2018). The temperature difference between water and air during CAOs can exceed 30 °C near the marginal sea ice zone, and the maximum values of the total turbulent heat flux can exceed 600 W/m^2 (Brümmer, 1996). As the air mass warms and moistens with increasing distance from the ice edge, the total heat flux decreases. The horizontal scale of the air mass transformation is about 500-1000 km for typical CAOs (Chechin and Lüpkes, 2017). Thus, large areas of the non-freezing seas, such as the Barents Sea, are subject to intense heat loss. The heat loss due to CAOs can reach up to 60% over the Greenland and Iceland Seas (Papritz and Spengler, 2017), although the specific value depends on the criteria used for the identification of CAOs. To our knowledge, no systematic study of the CAOs role in the air-sea heat

https://doi.org/10.5194/acp-2020-1007
Preprint. Discussion started: 28 October 2020

Atmospheric Chemistry and Physics Discussions

exchange exists for the Barents Sea, although the importance of CAOs has been stressed earlier (Smedsrud et al., 2013).

Furthermore, CAOs create favorable conditions for enhancing wind speed over water, which leads to further intensification of the energy exchange. The wind speed increase is primarily associated with the formation of large horizontal temperature gradients and strong baroclinicity. This can lead to the intensification of cyclones and mesocyclones (Kolstad, 2015), formation of jets and wind shear along the lower tropospheric fronts (Grønas and Skeie, 1999), convergence lines (Savijärvi, 2012), and low-level jets (Brümmer 1996; Chechin et al., 2013; Chechin and Lüpkes, 2019). Although the highest wind speeds over the Barents Sea have the orographic origin (e.g., the Novaya Zemlya Bora (Moore, 2013)), it was shown (Kolstad, 2015) that in cyclones, the wind speed reaches its maximum value when intense cold advection takes place in their rear part. In addition, intense turbulent exchange in the convective boundary layer effectively transports momentum down to the lower atmospheric layer increasing the near-surface wind speed (Chechin et al., 2015).

In this paper, we consider the influence of sea waves on turbulent heat fluxes in the Barents Sea. Heat fluxes were calculated using the COARE 3.0 algorithm and NCEP/CFSR reanalysis data with the Charnock roughness length parameterization and parameterizations explicitly taking into account the parameters of sea waves - Taylor and Yelland (2001), Oost et al. (2002) and Drennan et al. (2003). The results was verified by the ship measurements of turbulent heat fluxes obtained during the NABOS (Nansen and Amundsen Basins Observational System) campaigns in different years. The wind wave parameters were obtained from the WaveWatchIII (WWIII) wave model. Special attention is paid to the cases of intense storms and cold-air outbreaks events, when the expected difference between calculations with different roughness parameterizations is the largest.

2. Data and Methods

2.1 Wave modeling

The wave characteristics in the Barents Sea were computed using the spectral wave model WaveWatchIII (WWIII) version 4.18. The WW3 model is an development of the WAM model with regard to the functions of the source and the nonlinear interaction (Tolman, 2014). This model is based on a numerical solution of the equation of the spectral wave energy balance

$$\frac{\partial E(\omega, \theta, \vec{x}, t)}{\partial t} + \vec{V}(\omega, \theta)\nabla E = S(\omega, \theta, \vec{x}, t), \quad (1)$$

where ω and θ are the frequency and the propagation direction of the spectral component of the wave energy; $E(\omega, \theta, \vec{x}, t)$ is the two-dimensional spectrum of the wave energy at a point with vector coordinate $\vec{x}$ at time point t; $\vec{V}(\omega, \theta)$ is the group velocity of the spectral components; $S(\omega, \theta, \vec{x}, t)$ is a function that describes the wave energy sources and sinks, i.e., the transfer of the energy from the wind to the waves, nonlinear wave interactions, dissipation of the energy through collapse of the crests at a great depth and in the coastal zone, friction against the bottom and ice, wave scattering by ground relief forms, and reflection from the coastline and floating objects. The energy balance equation is integrated using finite-difference schemes by the geographic grid and the spectrum of wave parameters.

In this work, the computations were made using the ST1 scheme (Tolman, 2014). To account for the nonlinear interactions of the waves, the Discrete Interaction Approximation (DIA) model was used, which is a standard approximation for calculation of nonlinear interactions in all modern wave models.

https://doi.org/10.5194/acp-2020-1007
Preprint. Discussion started: 28 October 2020

To take into account ice effects on the wave development, the IC0 scheme was used, where the grid point is considered as ice-covered if the ice concentration was larger than 0.25. Thus, the exponential attenuation of wave energy adjusted for the sea ice concentration at a given point was added.

In the shallow water, the increase in wave height as waves approach the shore and the related wave breaking after waves reach the critical value of steepness were taken into consideration. The whitecapping effect taken into account in the ST1 scheme. The standard JONSWAP scheme was used to take the bottom friction into account. The spectral resolution of the model is 36 directions (Dq = 10°), the frequency range consists of 36 intervals (from 0.03 to 0.843 Hz).

The calculations were performed using the original unstructured grid, which is based on the bottom topography data from ETOPO1 database and detailed nautical charts (Figure 1). This unstructured grid consists of 16792 nodes; the spatial resolution varies from 15 km for the open part of the Barents Sea to 500 m for the coastal regions. The computational domain of the model covers the Barents and the Kara Seas and the entire northern part of the Atlantic Ocean (Figure 1). Previously, this grid was successfully used for wave modeling (Myslenkov et al., 2018; Myslenkov et al., 2019). The need to take into account the swell propagating from Atlantic ocean when calculating the height of significant waves in the Barents Sea was clearly shown in the previous work of the authors (Myslenkov et al., 2015).

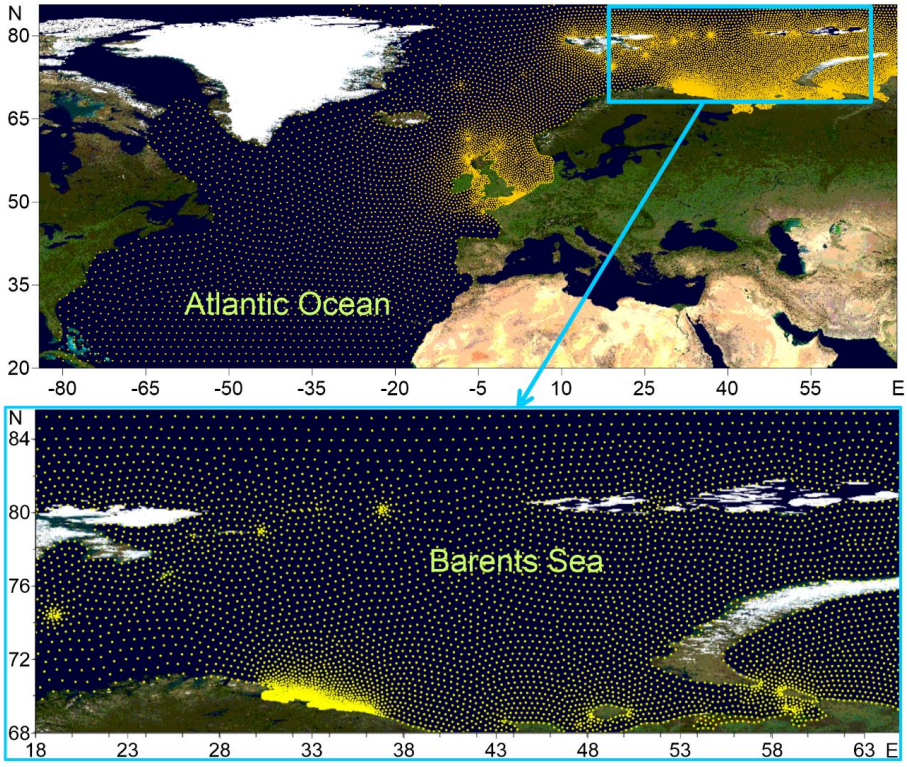

Figure 1. The computational unstructured grid for the Atlantic Ocean and the Barents Sea. The base map is the Blue Marble which obtained by connecting to the WMS demo server in the Surfer Golden Software program.

The general time step for the integration of the full wave equation was 15 minutes, the time step for the integration of functions of sources and sinks of wave energy was 60 s, the time step for the spectral energy transfer

https://doi.org/10.5194/acp-2020-1007
Preprint. Discussion started: 28 October 2020

Atmospheric Chemistry and Physics Discussions

and for satisfying the Courant–Friedrichs–Lewy condition was 450 s. This choice is dictated by the configuration of the computational grid: the maximum and minimum distances between the nodes and a large latitudinal extent.

The 10-m wind from the NCEP/CFSR reanalysis (Saha et al., 2010) for the period of 1979 to 2010 with the spatial resolution of ~0.3° was used as the forcing. Data of NCEP/CFSv2 reanalysis (Saha et al., 2014) with the resolution of ~0.2° and with the time step of 1 hour were used for the period of 2011 to 2017.

In this paper, we used the output results of the wave model with time step 3 hours from 1979 to 2017 for each node of the unstructured grid.

Based on the wave model results, a study of storm activity was carried out according to the POT (Peak Over Threshold) method which used successfully earlier in (Myslenkov et al., 2019). For each year in the Barents Sea, the number of storm surges with different significant wave heights from 5 to 8 m was calculated. The event is counted as the storm with wave height > 5 m if at least in one node in the study area the wave height exceeds the threshold of 5 m This event continues until the wave height at all nodes becomes less than the threshold. To eliminate possible errors, at least 9 hours should pass between two storm events. Using the described procedure, a catalog of storm days was compiled when the significant wave heights of more than 5 m were observed. A total of 1964 days were identified for the period 1979-2017.

2.2 COARE algorithm and parameterizing the roughness parameter

Turbulent heat fluxes were calculated using the COARE algorithm (Fairall et al., 1996), based on the LKB model (Liu et al., 1979). Bulk formulae for the momentum and scalar fluxes have the general form:

$$w'x' = c_x^{1/2} c_d^{1/2} S\Delta X = C_x S\Delta X, \quad (2)$$

where x is the horizontal wind components u, v, temperature or specific humidity, c_x – transfer coefficients for x, c_d – transfer coefficient for momentum, C_x – total transfer coefficient, ΔX – the difference the mean x at a height equal to the roughness length and at a certain height (10 m) in the atmospheric surface layer (Fairall et al., 2003). S – mean wind speed with gusts U_g:

$$S = \sqrt{U^2 + V^2 + U_g^2}$$

The default value of U_g is 0.5 m/s in the COARE algorithm. Transfer coefficients depend on the roughness length and dimensionless universal functions. The form of universal functions in the COARE algorithm is set in accordance with (Beljaars and Holtslag, 1991) for stable stratification; the so-called Kansas functions (Kaimal et al., 1972) are used for unstable stratification; functions from Fairall et al. (1996) and Grachev et al. (2000) are used for very unstable stratification. For the roughness length, several parameterizations are available in the COARE algorithm. The parameterization of Charnock (Charnock, 1955) implies dependence of roughness on the friction velocity u_*:

$$z_0 = \frac{\alpha u_*^2}{g} + \frac{0.11a}{u_*} \quad (3)$$

where α – Charnock parameter, g – gravity acceleration, a – kinematic viscosity coefficient (Andreas, 1989). Equation (3) is the modified Charnock formula (Smith, 1988), in which the second term on the right side describes the roughness over an aerodynamically smooth surface (i.e., in weak winds). The Charnock coefficient is set piecewise constant in strong and weak winds and linearly dependent on 10-m wind speed in moderate winds:

$$\begin{cases} 0.011, & S < 10\ m/s \\ 0.011 + \dfrac{0.007(S-10)}{8}, & 10\ m/s < S < 18\ m/s \\ 0.018, & S > 18\ m/s \end{cases}$$

https://doi.org/10.5194/acp-2020-1007
Preprint. Discussion started: 28 October 2020

Atmospheric Chemistry and Physics Discussions

In the parameterization of Taylor and Yelland (2001) (hereafter - T1), the roughness length is related to the wave steepness (H_s/L_p):

$$z_0 = H_s a_1 \left(\frac{H_s}{L_p}\right)^{b_1} + \frac{0.11a}{u_*}, \quad a_1 = 1200, \quad b_1 = 4.5 \tag{4}$$

where H_s – significant wave height, L_p – spectral peak wavelength.

The parameterization of Oost et al. (2002) (hereafter - O2) implies the dependence of the roughness length on the spectral peak wavelength L_p and inverse wave age (U_*/c_p):

$$z_0 = L_p a_2 \left(\frac{u_*}{c_p}\right)^{b_2} + \frac{0.11a}{u_*}, \quad a_2 = 50/2\pi, \quad b_2 = 4.5 \tag{5}$$

Here c_p –phase wave speed associated with spectral peak, which is expressed through the wave length as $c_p = \sqrt{L_p g/2\pi}$.

Finally, we included the parametrization of Drennan et al. (2003) (hereafter - D3) in the COARE algorithm. D3 parameterization consists in the dependence of the roughness length on the wave height and inverse wave age:

$$z_0 = H_s a_3 \left(\frac{u_*}{c_p}\right)^{b_3} + \frac{0.11a}{u_*}, \quad a_3 = 3.35, \quad b_3 = 3.4 \tag{6}$$

Thus, the main components of the algorithm are the equation (2), formulae for calculating transfer coefficients based on the Monin-Obukhov similarity theory, and formulae (3-6) for the roughness length. Thus, in general, the COARE algorithm is similar to corresponding algorithms in most atmospheric models.

Using the COARE algorithm, we calculated turbulent sensible and latent heat fluxes in the Barents Sea from 1979 to 2017. Mean fluxes were calculated for long-term period and for periods of cold-air outbreaks and storm wave events.

2.3 Input data for the COARE algorithm

Input data for the COARE algorithm are: wind vector, air temperature, sea surface temperature (SST), air humidity, incoming short-wave and long-wave radiation, precipitation intensity, sea wave height and period. NCEP/CFSR and CFSv2 (Saha et al., 2010, 2014) reanalysis with temporal resolution of 6 hours and total period 1979-2017 were used as atmospheric data input for the COARE algorithm . CFSv2 reanalysis data for the period 2011-2017 (with a slightly better spatial resolution than CFSR, were interpolated from the ~0.2˚ grid to ~0.3˚ grid to match the CFSR resolution. The wind speed was used at 10 m height, air temperature and humidity were used at 2 m height. Reanalysis data are also available at isobaric levels, the lower of which is 1000 hPa. However, we preferred to take diagnostic variables at heights of 2 and 10 m for several reasons. Firstly, the height of the isobaric levels varies greatly and the lower available level may be at a high height (above the boundary layer). Secondly, data at vertical levels are available on a much coarser grid (0.5 °). For instance, Arthun and Schrum (2010) also used diagnostic variables at standard levels from the NCEP-NCAR reanalysis to calculate turbulent fluxes in the ocean model. The surface pressure and the inversion height (boundary layer height), which are usually set constant in the COARE algorithm, were set from the CFSR reanalysis (at each moment of time and at each grid point).

2.4 Ship observations

https://doi.org/10.5194/acp-2020-1007
Preprint. Discussion started: 28 October 2020

Atmospheric Chemistry and Physics Discussions

We used ship observations in the Barents Sea from the NABOS expeditions in 2005, 2007, 2013, and 2015 to verify turbulent heat fluxes calculated using the COARE algorithm. All expeditions took place in a period from August to October. Ship-borne fluxes were calculated using the eddy-covariance method (the left side of equation (2)) based on high-frequency measurements of temperature and the three wind components using Gill and Metek sonic anemometers (Ivanov et al., 2019; Varentsov et al., 2016). The averaging period for the covariance calculations was 10 min. For all wind measurements, a correction was made for the movement of the ship. A detailed description of the location of the instruments and methods of filtering data and calculating fluxes is available at https://uaf-iarc.org/nabos-cruises/. For verification, the calculated values of heat fluxes were bilinearly interpolated from the CFSR reanalysis grid to the observation points.

2.5. Identification of CAOs

The so-called «CAO index» is frequently used for CAO identification. It was first defined (Kolstad and Bracegirdle, 2008; Kolstad et al., 2009) as the potential temperature difference between the ocean surface and the 700 hPa height normalized by the pressure difference at the same heights. The authors used the value of the 90th percentile of the CAO index to estimate the strength and frequency of occurrence of CAOs. Other investigators (e.g., Fletcher et al., 2016) used the non-normalized potential temperature difference between the surface and the 800hPa height. As metrics to study the frequency and strength of CAOs they evaluated the frequency of occurrence of the positive values of the CAO index, as well as the value of the 95th percentile of the CAO index during the winter months.

Here, we define the CAO index I_{cao} as the daily potential temperature difference between the ocean surface and the 700 hPa height. For each day, I_{cao} was averaged over the ice-free part of the Barents sea. Figure 2 shows the obtained I_{cao} values for the period 1979-2018. Solid curve on Figure 2 consists of the multiyear-averaged values $\overline{I_{CAO}}$ obtained by 1) averaging I_{cao} over a 30-day period centered on the given day and 2) averaging the obtained values over the years. Similarly, the standard deviation σ_I of I_{cao} was obtained.

https://doi.org/10.5194/acp-2020-1007
Preprint. Discussion started: 28 October 2020

Atmospheric Chemistry and Physics Discussions

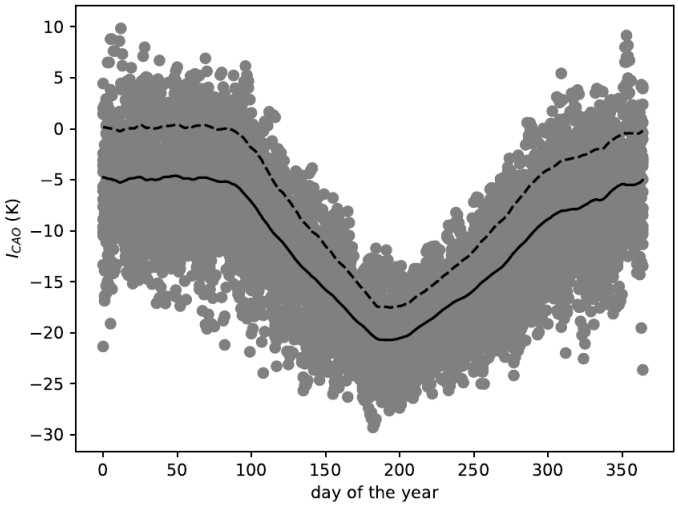

Figure 2. Cold-air outbreak index I_{cao} for the period 1997-2017. Solid curve represents the 30-day running multiyear mean values $\overline{I_{CAO}}$. Extreme CAOs correspond to points above the dashed curve which is the sum $\overline{I_{CAO}} + \sigma_I$ where the latter is the 30-day running multiyear standard deviation of I_{cao}.

The dashed curve in Figure 2 represents the threshold value $\overline{I_{CAO}} + \sigma_I$ which we use as a criteria for CAO identification, namely

$$I_{CAO} > \overline{I_{CAO}} + \sigma_I \qquad (7)$$

According to the criteria (7), we identify CAOs as those cases when I_{cao} values are above the dashed curve in Figure 2. A similar procedure was used in other studies (e.g., Wheeler et al., 2011) to identify continental CAOs where authors used simply the air temperature at 2 m height instead of I_{cao}.

Figure 2 shows that the largest values of I_{cao} are observed in a period from the second half of December until the end of March when the coldest air advection occurs over the Barents Sea. It is interesting to note that in winter the criteria (7) is almost identical to simply $I_{cao} > 0$. The latter serves as a measure of the dry hydrostatic stability of the layer between the ocean surface and the 700 hPa surface. Thus, positive values of I_{cao} indicate conditions favorable for the mixed-layer development to the heights over 700 hPa. During strong background advection mixed-layer can reach such heights only at a significant distance from the ice edge (Chechin and Lüpkes, 2017).

3. Results

3.1 Wave climate and storm activity

First, we consider the main features of wave conditions and wave climate in the Barents Sea, which directly affect the processes of heat exchange in the ocean-atmosphere system. In Figure 3 the average significant wave heights for the entire simulation period from 1979 to 2017 is shown. The highest average wave heights are found in the western part of the sea. Here we can expect the greatest influence of sea waves on heat fluxes. In the north, due to the presence of ice, the average wave heights do not exceed 1 m.

https://doi.org/10.5194/acp-2020-1007
Preprint. Discussion started: 28 October 2020

Atmospheric Chemistry and Physics Discussions

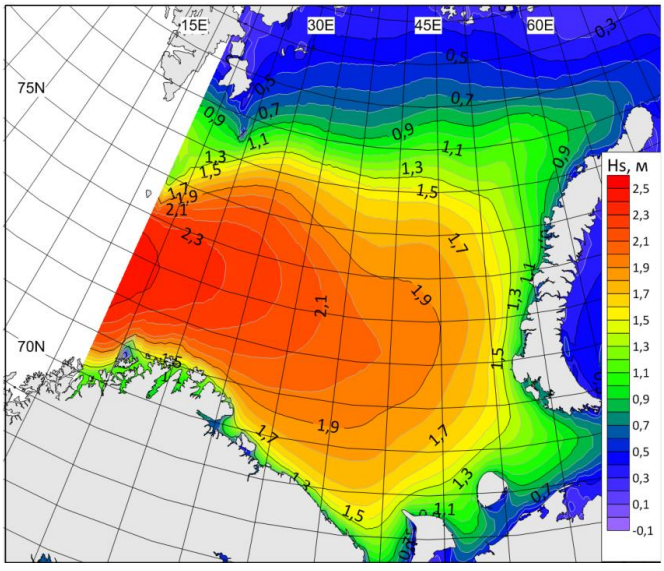

Figure 3. Long-term average significant wave height in the Barents Sea based on the WWIII simulation results for the period 1979-2017.

Also, an equally important parameter is the wavelength, which is used in the parametrizations O2 and D3. In Figure 4 the mean long-term spectral peak wavelength is shown. The wavelengths 80-100 m are observed in the central and western parts of the Barents Sea. The results on the average wave height and wavelength in general are consistent with similar works by other authors (Semedo et al., 2011; Stopa et al., 2016). Estimates of storm activity based on such long-term analysis are relatively rare and their detailed analysis is necessary an additional research.

https://doi.org/10.5194/acp-2020-1007
Preprint. Discussion started: 28 October 2020

Atmospheric Chemistry and Physics Discussions

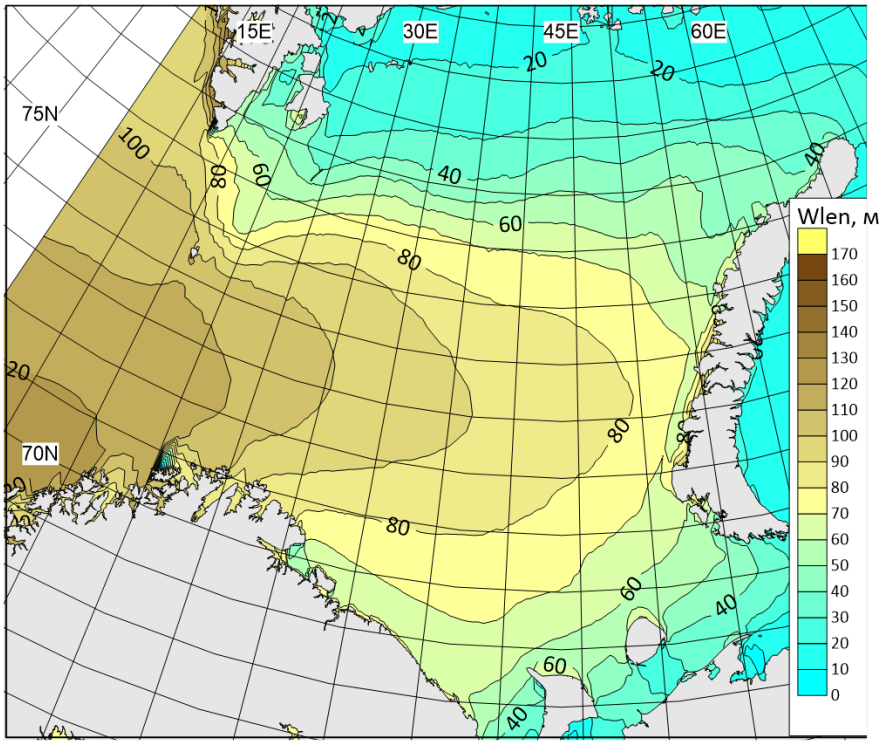

Figure 4. Long-term average long-term spectral peak wavelength in the Barents Sea based on the WWIII simulation results for the period 1979-2017.

The Barents Sea is characterized by a high frequency of storm wave events, which provide a long swell in the extinction stage (i.e., “old seas”) and limit the applicability of the Charnock formula. As shown in (Myslenkov et al., 2018), the number of storms per year in the Barents Sea can differ significantly. Figure 5 shows the number of storms calculated according to the wave model results with wave heights of more than 5 m and more than 7 m (identified as described in the Section 2.1). During the period from 1979 to 2017, several maxima of storm activity were observed, for example, in 1989-1991 and in 2011. Especially for these periods, the calculated heat fluxes are expected to be sensitive to the used of parameterizations of the roughness length (see Section 3.5).

https://doi.org/10.5194/acp-2020-1007
Preprint. Discussion started: 28 October 2020

Atmospheric Chemistry and Physics Discussions

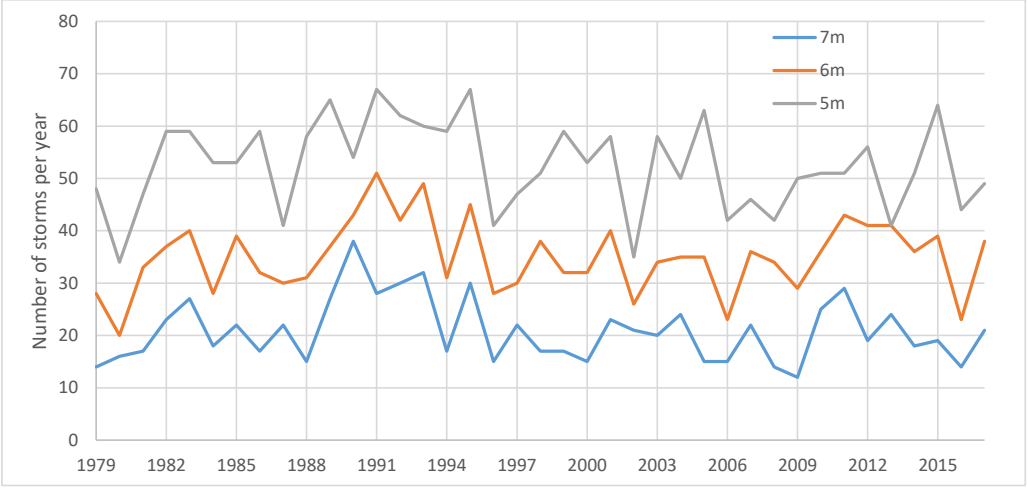

Figure 5. The number of storms with a significant wave height of more than 5, 6 and 7 m according to the WWIII simulation results for the period 1979-2017.

3.2 CAOs frequency of occurrence

Figure 6 shows the timeseries of the number of days with extreme CAOs selected using criteria (7) for each cold period (November-April) of 1979-2018. On average, CAOs are observed in 16.4 % days. However, the interannual variability of the frequency of occurrence of CAOs is large. Namely, the interannual standard deviation of the number of CAO days amounts to 12 days. Thereby, the number of CAO days per cold season varies from 6 in 2011-2012 to 56 in 1980-1981.

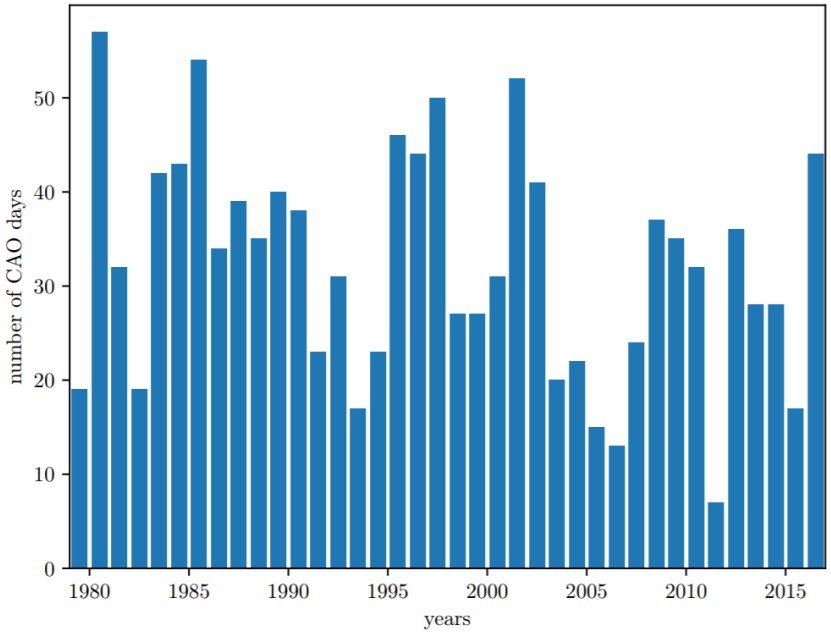

Figure 6. The number of days with CAOs over the Barents Sea selected using criteria (7) for each cold season in 1979-2018.

https://doi.org/10.5194/acp-2020-1007
Preprint. Discussion started: 28 October 2020

Atmospheric Chemistry and Physics Discussions

341 The frequency of occurrence of CAOs over the Barents Sea is governed by the variability of the largescale
342 patterns of atmospheric circulation. To the largest extent, the frequency of CAOs is correlated with the so-called
343 «Barents Oscillation» (Skeie et al., 2000; Wu et al. 2006; Kolstad et al., 2009). The latter is the mode of variability of
344 the sea-level pressure field represented by a dipole with high pressure over Greenland and Iceland and low pressure
345 over the northern part of the European part of Russia. Such pressure field promotes intense cold-air advection over the
346 Barents Sea from the north. Moreover, there is a negative correlation between the North Atlantic Oscillation index and
347 CAOs frequency of occurrence (Kolstad et al., 2009). Such a correlation is particularly strong for easterly CAOs,
348 which is obviously associated with the reduced strength of the westerlies.

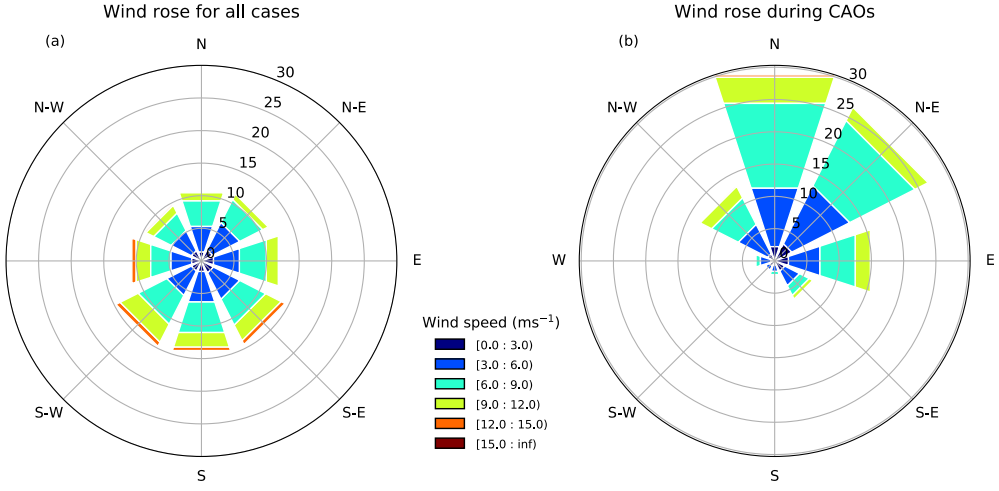

349
350
351 Figure 7. Frequency of occurrence of daily 10 m wind speed and direction, averaged over the ice-free part of
352 the Barents Sea for the period November-April 1979-2018 for all cases (a) and cold-air outbreaks (b).
353

354 The frequency of CAOs with easterly wind over the Barents Sea is significant and amounts to 16% of all
355 CAOs (Figure 7b). During CAOs, the highest frequency of occurrence have northerly (30%) and north-easterly (27%)
356 winds. The wind rose in CAOs differs from the wind rose in all cases during the cold season (Figure 7a). In particular,
357 the prevailing wind direction over the Barents sea in winter is from the south. Moreover, the winds having southerly
358 and westerly components are the strongest.
359 The CAOs role in the heat exchange between the Barents Sea and the atmosphere is demonstrated by Figure
360 8. The latter shows the turbulent fluxes of sensible and latent heat, H and LE, respectively, the net longwave radiative
361 flux LW_{net}, and the total heat flux $F_{total} = H + LE + LW_{net}$ averaged over the November-April period over the ice-
362 free part of the Barents Sea as functions of the number of CAO days during the same period. Clearly, there is a strong
363 dependency of the Barents Sea on the number of CAO days. The highest correlation coefficients are obtained for
364 LW_{net}, F_{total} and H amount to 0.86, 0.85 and 0.84, respectively. A smaller correlation coefficient of 0.78 is obtained
365 for LE. Also, the coefficients of linear regression shown in Figure 8 demonstrate that F_{total} has the strongest
366 dependency on the number of CAO days. From all terms of the surface heat balance, the sensible heat flux H is most
367 sensitive to the number of CAO days. All the three considered components of the surface heat balance (H, LE and
368 LW_{net}) manifest heat loss from the sea surface to the atmosphere and are of comparable magnitude of about 70 Wm^{-2}
369 on average.

https://doi.org/10.5194/acp-2020-1007
Preprint. Discussion started: 28 October 2020

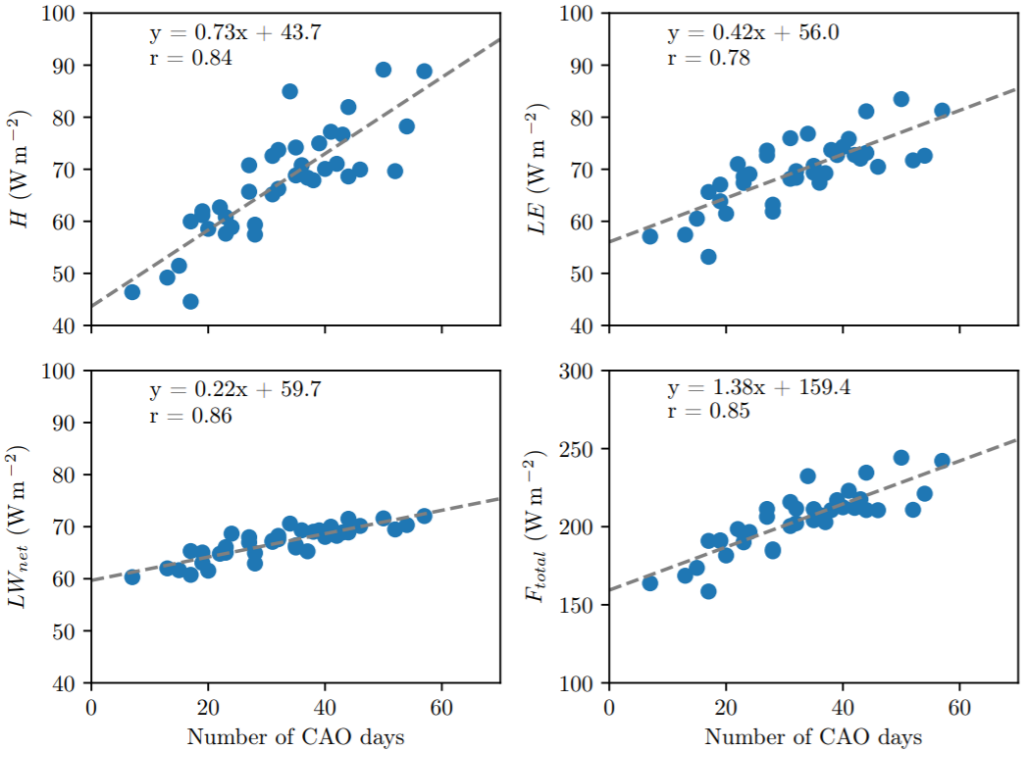

Figure 8. Turbulent fluxes of sensible and latent heat, H и LE respectively, net longwave radiative flux LW_{net} and the total heat flux $F_{total} = H + LE + LW_{net}$ averaged over the cold season (November-April) and over the ice-free part of the Barents Sea as function of number of CAO days during the same period for 1979-2018. Dashed line shows the linear regression line, whose equation is given at each plot, as well as the correlation coefficient r.

We stress that the values of fluxes shown in Figure 8 are averaged over the ice-free part of the Barents Sea. It is important to keep in mind that there is a large interannual variability of the area of sea ice cover in the Barents Sea. This is another important factor, along with the number of CAO days, influencing the heat loss.

3.3 Verification of the COARE algorithm by the ship observations

Figure 9 shows the comparison of sensible and latent heat fluxes from shipborne observations and calculated using different roughness parameterizations, namely Charnock, 1955 (C55), Taylor and Yelland, 2001 (T1), Oost et al., 2002 (O2) and Drennan et al., 2003 (D3).

https://doi.org/10.5194/acp-2020-1007
Preprint. Discussion started: 28 October 2020

Atmospheric Chemistry and Physics Discussions

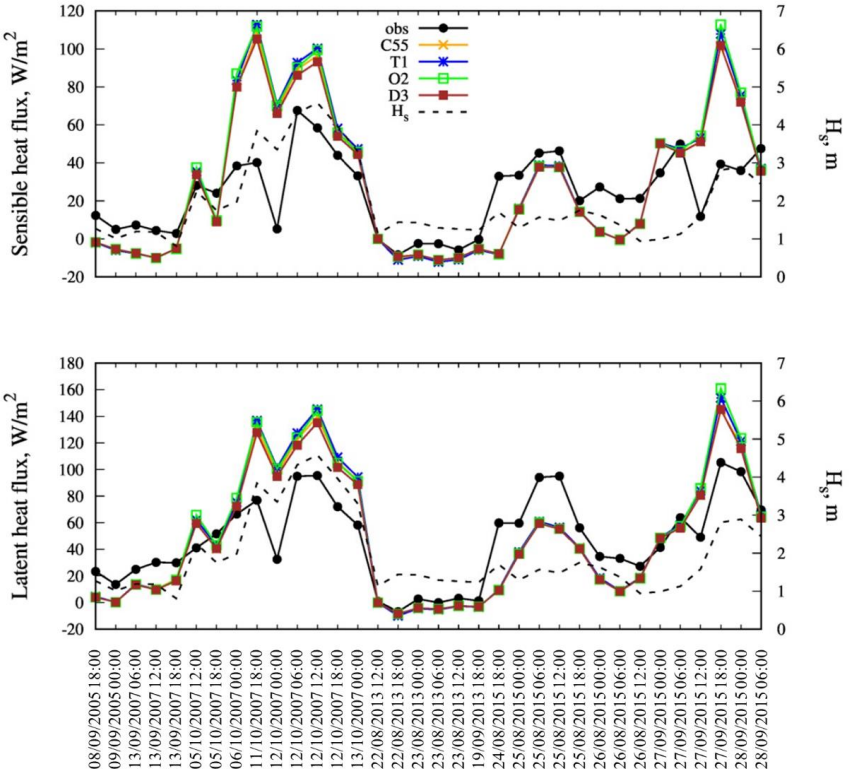

Figure 9. Sensible (top) and latent (bottom) heat fluxes according to NABOS observations and calculated using various roughness parameterizations. The dashed line shows the significant wave height H_s according to WWIII simulations.

Heat fluxes calculated with different roughness parameterizations are almost identical (Figure 9); an average difference between them is 1 W m^{-2}. The correlation coefficient between the observed and the calculated fluxes is 0.7 for the sensible heat flux and 0.8 for the latent heat flux. However, the mean absolute error (MAE) is rather large - about 20 W m^{-2}. The error magnitude increases with the increase of the heat flux magnitude. The error may be connected both with the COARE algorithm itself and with the input data (i.e., related to the quality of meteorological parameters in the reanalysis). For example, a strong overestimation of heat fluxes on October 11–12, 2007 is associated with the overestimation of wind speed (by 6–8 m s^{-1}) compared to observations.

In order to estimate the accuracy of the COARE algorithm itself, we excluded from the analysis those samples for which the reanalysis errors were large, namely, when the wind speed error exceeded 4 m s^{-1} and/or the SST and air temperature error exceeded 1.5 °C and/or the error in specific humidity exceeded $0.7 \cdot 10^{-3}$ kg kg^{-1}. For such a sample, MAE decreased by half, to 10 W m^{-2}. For those periods when the error of wind speed, temperature, and specific humidity was the smallest, an error in the resulting heat fluxes also becomes small and amounts to about 5 W m^{-2}, which is most likely associated with the inaccuracy of the COARE algorithm. However, this error is within the accuracy of the eddy-covariance method. The accuracy of this method in the case of ship measurements can be significantly reduced due to the influence of air flow distortion by the ship. Therefore, we can conclude that the

https://doi.org/10.5194/acp-2020-1007
Preprint. Discussion started: 28 October 2020

Atmospheric Chemistry and Physics Discussions

404 calculated fluxes are in good agreement with the observations. It should be noted that the error between the observed
405 and calculated fluxes for all parameterizations exceeds the difference between calculated fluxes using different
406 parameterizations.
407
408 **3.4 Long-term mean turbulent heat fluxes**
409 Here we consider the mean long-term values of heat fluxes calculated from the CFSR reanalysis data using
410 COARE algorithm and various roughness parameterizations. The mean (for the period 1979-2017) sensible and latent
411 heat flux in the experiment C55 and difference in the between different experiments shown on Figure 10, 11. The
412 main conclusion of these results is the presence of positive difference for T1 and O2 experiments and negative for D3.
413 The long-term values of difference is small: 1-2 W m^{-2} for T1 and 0.5-1 W m^{-2} for O2.

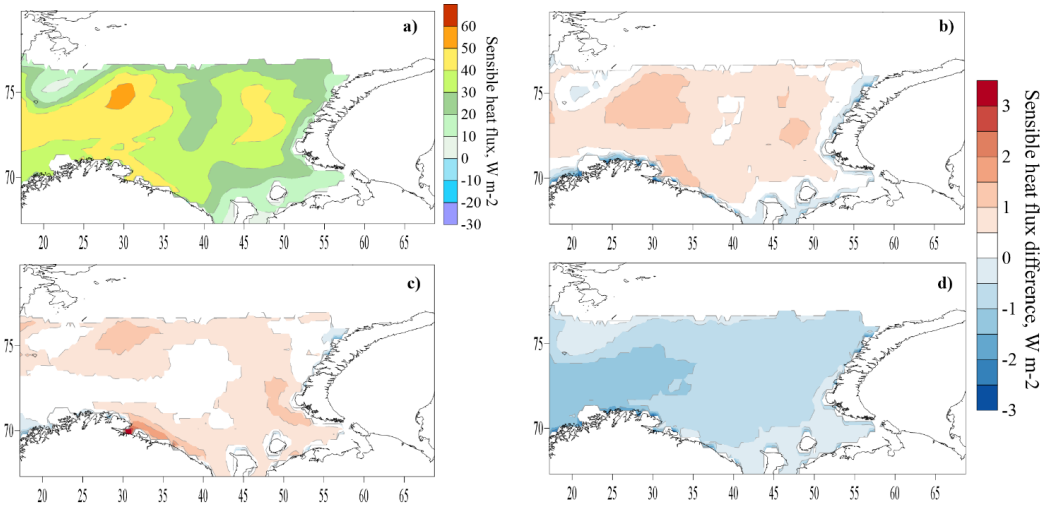

414
415 Figure 10. Mean sensible heat flux in the experiment C55 (a,) and the difference in the sensible heat fluxes
416 between experiments T1 - C55 (b), O2 - C55 (c) and D3 - C55 (d). All grid nodes where sea ice was in more than half
417 of the cases are filtered.

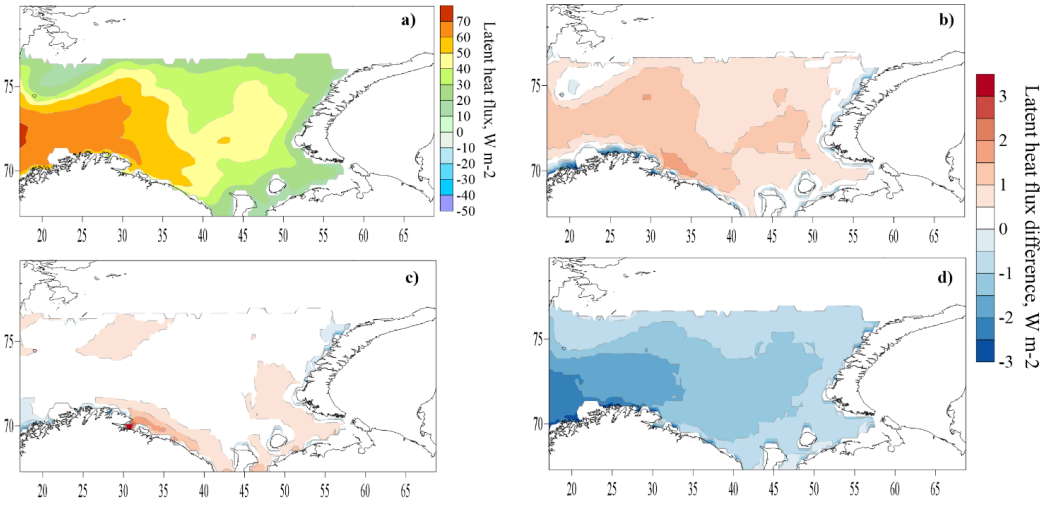

418

https://doi.org/10.5194/acp-2020-1007
Preprint. Discussion started: 28 October 2020

Atmospheric Chemistry and Physics Discussions

Figure 11. Mean latent heat flux in the experiment C55 (a,) and the difference in the latent heat fluxes between experiments T1 - C55 (b), O2 - C55 (c) and D3 - C55 (d). All grid nodes where sea ice was in more than half of the cases are filtered.

Tables 1, 2 show the average statistics: the difference in heat fluxes with and without explicit accounting for sea waves parameters. Over the entire Barents Sea, the full range of differences in the fluxes are small, within -3 ÷ 2 W m^{-2}, which is only 1-3% of the mean absolute value. The greatest mean difference for sensible heat flux observed for T1 and for latent heat flux for O2 parametrization.

The flux difference can exceed 30-50 W m^{-2} (in 0.1% of cases or 99.9 percentile) and in some extreme cases reach 100-250 W m^{-2}. The highest maxima of the flux difference are obtained for the experiment O2.

Table 1

Statistical characteristics of the difference in the sensible heat flux calculated with and without explicit accounting for sea waves parameters: mean difference, relative mean (ratio of the mean difference to the mean value of the flux), mean absolute difference, 95 and 99.9 percentile and the maximum difference for the Barents Sea

	Mean difference (W m^{-2})	Relative mean difference (%)	Mean absolute difference (W m^{-2})	95 percentile (W m^{-2})	99.9 percentile (W m^{-2})
T1 - C55	0.5	1.4	1.7	7.3	40
O2 - C55	0.6	2.1	1.6	6.7	56
D3 - C55	-0.7	-2.3	1.1	3.7	35

Table 2

Statistical characteristics of the difference in the latent heat flux calculated with and without explicit accounting for sea waves: mean, relative mean (ratio of the mean difference to the mean value of the flux), mean absolute difference, 95 and 99.9 percentile and the maximum difference for the Barents Sea

	Mean difference (W m^{-2})	Relative mean difference (%)	Mean absolute difference (W m^{-2})	95 percentile (W m^{-2})	99.9 percentile (W m^{-2})
T1 - C55	0.7	1.6	1.8	6.7	41
O2 - C55	0.6	1	1.7	6.4	50

https://doi.org/10.5194/acp-2020-1007
Preprint. Discussion started: 28 October 2020

D3 - C55	-1.1	-2.8	1.3	3.7	38

The greatest differences between the experiments are found in those areas where the highest values of the heat fluxes are observed. This can be explained by the power-law dependence of the roughness length on the friction velocity / wave height. Moreover, in the O2 parameterization, the proportionality coefficient is larger (a2 = 4.5) than in the D3 parameterization (a3 = 3.4), which is reflected in the flux differences.

A more detailed spatial analysis of 99.9 percentile of sensible heat flux difference shown on Figure 12. The extreme values of the flux difference taking O2-C55 difference as an example showed that some of the extrema are associated with coastal areas, mainly off the western coast of Novaya Zemlya during bora. Other extremes were associated with deep cyclones in different parts of the sea, with different distances from the coast. Some extremes are associated with storm waves or are observed immediately after storms, during cold-air outbreaks in the rear of cyclones. Therefore, the characteristics of heat fluxes during storm waves and cold-air outbreaks will be considered separately in the following sections.

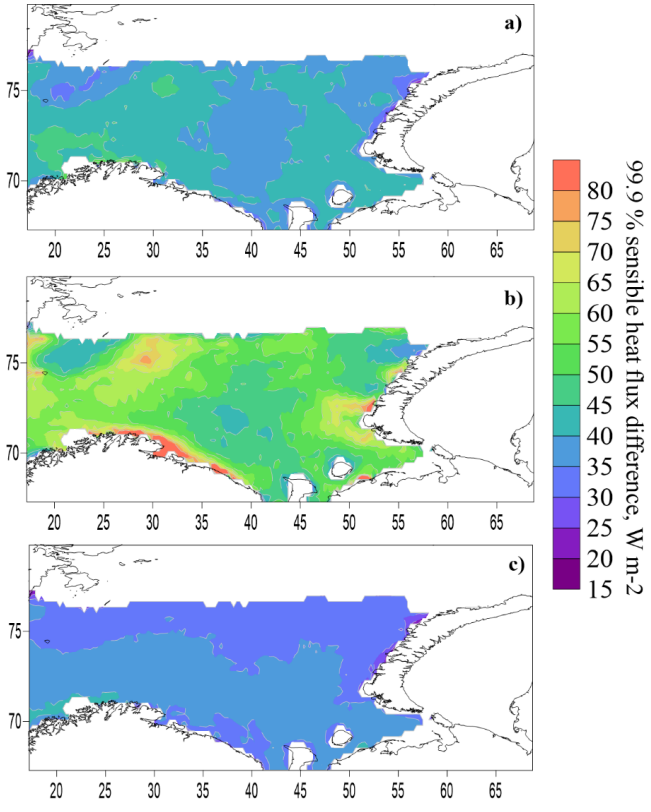

Figure 12. 99.9 percentile of sensible heat flux difference between experiments T1 - C55 (a), O2 - C55 (b) and D3 - C55 (c)

3.5 Turbulent heat fluxes during storm wave events

Here we consider turbulent heat fluxes during the storms identified in Section 3.1 (a total of 1964 days with storms for the period 1979-2017). The spatial distribution of heat fluxes during storms (Figure 13, 14) resembles the

https://doi.org/10.5194/acp-2020-1007
Preprint. Discussion started: 28 October 2020

Atmospheric Chemistry and Physics Discussions

458 average distribution (Figure 10, 11), but the absolute values increase by almost a factor of 2. The average sensible
459 heat flux has several maxima - in the northwest of the sea, near the coast of the Kola Peninsula and a less pronounced
460 local maximum off the southern island of Novaya Zemlya. The flux difference between the experiments is also
461 distributed the same as on average and increases in absolute value (except for experiment D3). The average flux
462 difference between experiments reaches 4-5 W m^{-2} for T1-C55, 8 W m^{-2} for O2-C55 and 3-4 W m^{-2} for D3-C55. On
463 average, the relative difference in heat fluxes is 3% for T1-C55 and 3-5% for O2-C55. The correlation coefficient
464 between the magnitude of the flux and the magnitude of the flux difference is 0.9. For the D3 experiment, the flux
465 difference gradually increases from east to west, and some special structure associated precisely with storms does not
466 appear. The detected maxima of flux difference in the western part of Sea generally correspond to the maxima of the
467 average wave height (Figure 3).
468 It can be concluded that the mean pattern of heat fluxes in the Barents Sea is largely contributed by storms.

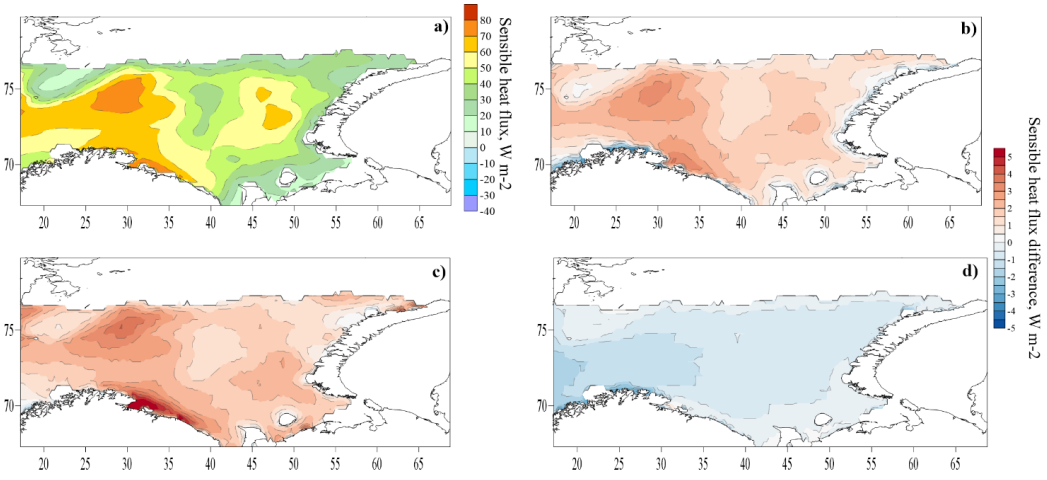

469
470 Figure 13. Mean sensible heat flux in experiment C55 (a) and the flux difference in experiments T1 - C55
471 (b), O2 - C55 (c) and D3 - C55 (d) during storms.
472

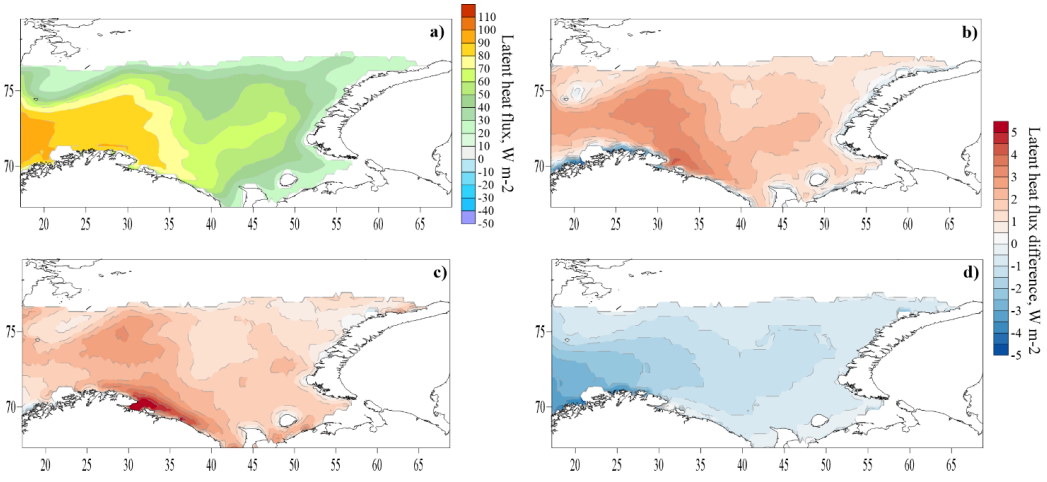

473
474 Figure 14. Mean latent heat flux in experiment C55 (a) and the flux difference in experiments T1 - C55 (b),
475 O2 - C55 (c) and D3 - C55 (d) during storms.
476

https://doi.org/10.5194/acp-2020-1007
Preprint. Discussion started: 28 October 2020

Atmospheric Chemistry and Physics Discussions

3.6 Turbulent heat fluxes during the cold-air outbreaks

Here we consider turbulent heat fluxes during cold-air outbreaks identified in Section 3.2 (2326 days with cold-air outbreaks for the period 1979-2017). The average values of the sensible heat flux increase, especially in the northwestern part (2 times compared with the average), during cold-air outbreaks (Figure 15a). The spatial distribution of the latent heat flux is almost the same with the average one, but the flux magnitude increases by 1.5 times (Figure16a).

Experiments T1 and O2 everywhere provide to increase the magnitudes of the sensible and latent heat fluxes compared to C55 during cold-air outbreaks (Figure 15, 16). Explicit accounting for the storm wave events leads to an increase in heat fluxes mainly in the northwest of the sea and near the ice edge. But the differences between the experiments are still small - on average less than 4 W m $^{-2}$ for the sensible heat flux and less than 2.5 W m^{-2} for the latent heat flux, i.e. less than 3-4% of flux magnitudes (Figure 15, 16). At the same time, the extreme values of the flux difference during cold-air outbreaks, as for storm waves, are several times smaller than when considering long-term means.

The average values of the flux difference during cold-air outbreaks are smaller than during storms, but the extreme values during cold-air outbreaks and during storms are close.

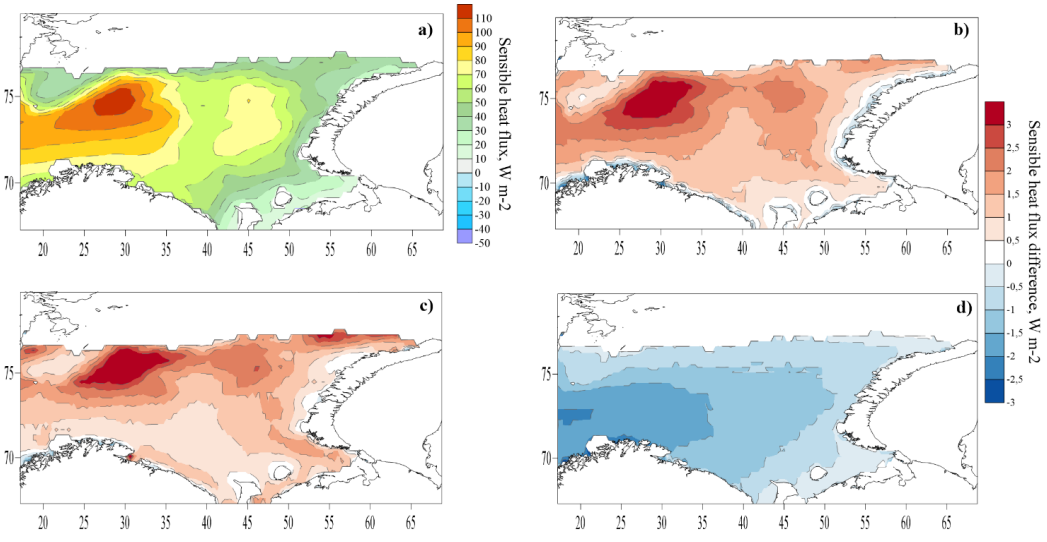

Figure 15. Mean sensible heat flux in experiment C55 (a) and the flux difference in experiments T1 - C55 (b), O2 - C55 (c) and D3 - C55 (d) during cold-air outbreaks.

https://doi.org/10.5194/acp-2020-1007
Preprint. Discussion started: 28 October 2020

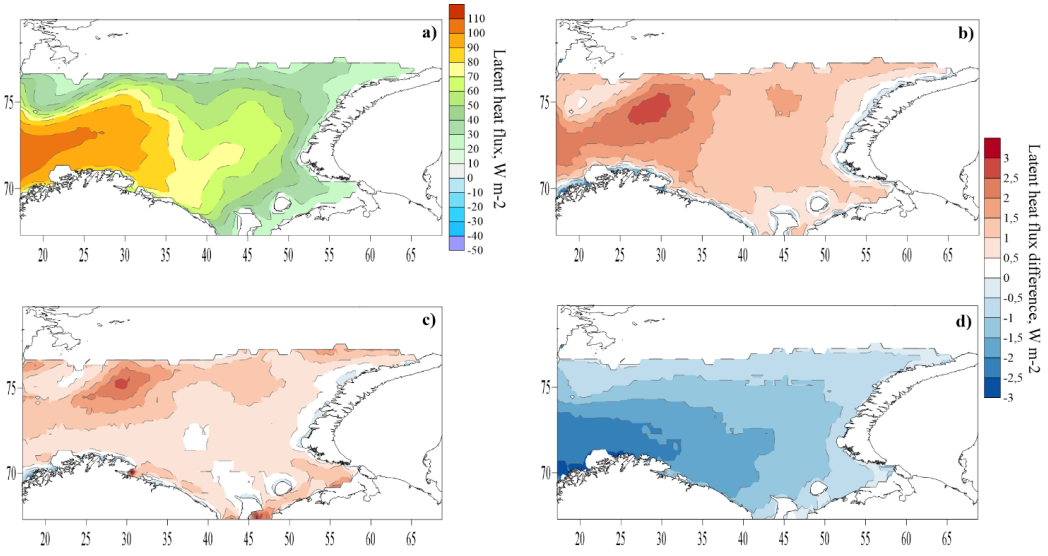

Figure 16. Mean latent heat flux in experiment C55 (a) and the flux difference in experiments T1 - C55 (b), O2 - C55 (c) and D3 - C55 (d) during cold-air outbreaks.

3.7 Turbulent heat fluxes during the simultaneously observed storm waves and cold-air outbreaks

Finally, we consider cases when cold-air outbreaks and storm wave events were simultaneously observed (a total of 292 days for the period 1979-2017) (Figure 17, 18). The magnitude of the heat fluxes and the difference between the experiments in these cases are the largest in comparison with other situations. The sensible heat flux in experiment C55 reaches 170 W m^{-2} (in the north-west of the sea), the latent heat flux is 140 W m^{-2} (in the west). The average difference T1-C55 reaches 6 W m^{-2} for sensible heat flux and 4.5 W m^{-2} for latent heat flux. The average difference O2-C55 reaches 10 W m^{-2} for sensible heat flux and 7 W m^{-2} for latent heat flux. The average difference D3-C55 reaches 3 W m^{-2} in the west of the sea.

The extreme values of the difference, which can reach 700 W m^{-2}, are also greatest in the case of simultaneously observed storms and cold-air outbreaks. Figure 19 shows case when the difference in sensible heat fluxes exceeded 100 W m^{-2} between C55 and T1 parametrizations and 400 W m^{-2} between C55 and O2 parametrizations. The greatest difference is noted for the eastern local maximum of the heat flux associated with the cold-air outbreak during the north-eastern wind. An analysis of other cases, in which extreme values of the flux difference were observed, also showed the presence of two local maxima (western and eastern) of heat fluxes. The same maxima also appear in the long-term mean pattern of heat fluxes (Figure 15, 16).

https://doi.org/10.5194/acp-2020-1007
Preprint. Discussion started: 28 October 2020

Atmospheric Chemistry and Physics Discussions

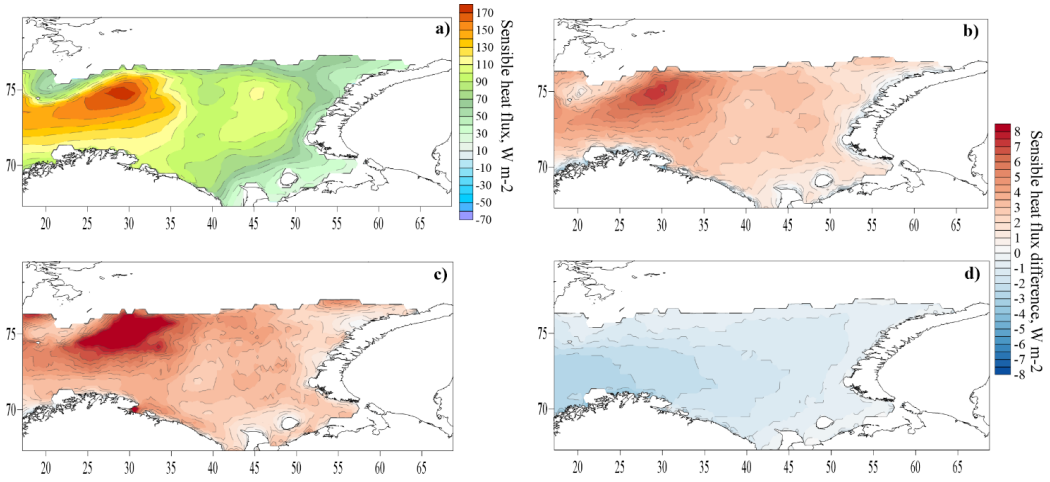

Figure 17. Mean sensible heat flux in experiment C55 (a) and the flux difference in experiments T1 - C55 (b), O2 - C55 (c) and D3 - C55 (d) during storms and cold-air outbreaks.

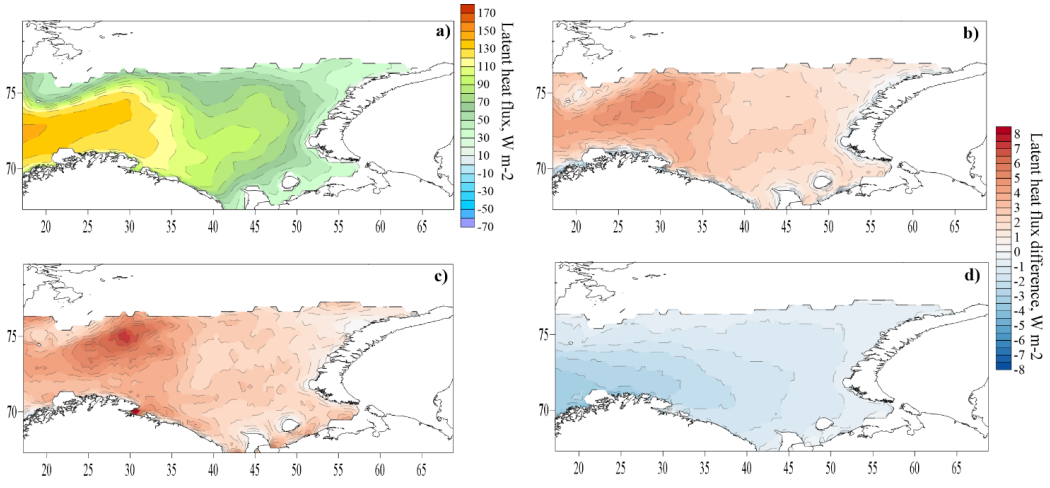

Figure 18. Mean latent heat flux in experiment C55 (a) and the flux difference in experiments T1 - C55 (b), O2 - C55 (c) and D3 - C55 (d) during storm waves and cold-air outbreaks.

https://doi.org/10.5194/acp-2020-1007
Preprint. Discussion started: 28 October 2020

Atmospheric Chemistry and Physics Discussions

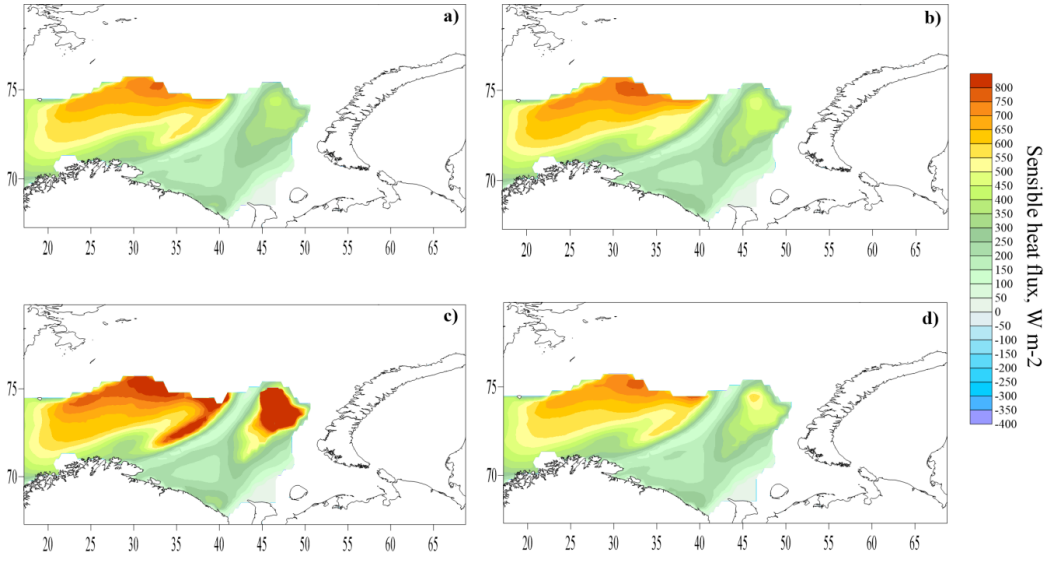

Figure 19. Sensible heat fluxes at 00 UTC January 13, 2003 calculated with C55 (a), T1(b), O2(c) and D3(d) parametrizations.

4. Discussion and conclusions

This paper presents the results of turbulent heat flux calculations in the Barents Sea using the COARE algorithm, meteorological data from reanalysis and sea-wave data from retrospective simulations with the WW3 wave model. The calculations were performed for several options: using the modified Charnock parameterization of roughness length (C55) and using the explicit accounting for the sea waves parameters in the roughness parametrizations T1 (Taylor and Yelland), O2 (Oost et al.) and D3 (Drennan et al.). Particular attention was paid to the episodes with extremely intense energy exchange between the atmosphere and the ocean: storms and cold-air outbreaks (CAOs).

We obtained the mean annual distribution of the height and wavelength in the Barents Sea from wave modelling results. Estimates of the storm activity from 1979 to 2017 were also obtained, confirming its high interannual variability. Based on the data of wave modeling, a catalog of storm waves with the wave height exceeding 5 m was created. This catalog was used to calculate heat fluxes during storms.

The catalog of extreme CAOs over the Barents Sea was also obtained. It is shown that the extreme CAOs are observed in 16.4% of days of a cold season (November-April). However, the number of CAO days varies from 6 in 2011-2012 to 56 in 1981-1982 manifesting large interannual variability. The important role of CAOs in the energy exchange of the Barents Sea and the atmosphere is demonstrated. A high correlation was found between the number of CAO days and turbulent fluxes of sensible and latent heat, as well as with the net flux of long-wave radiation averaged over the ice-free surface of the Barents Sea during a cold season. Thus, the significant interannual variability of the frequency of occurrence of CAOs largely determines the interannual variability of heat loss from the ice-free surface of the Barents Sea.

Comparison of the calculated heat fluxes with ship observations during the NABOS expeditions was carried out. Significant part of the errors in determining the heat fluxes is associated not with the used COARE algorithm, but with discrepancies in meteorological parameters reproduced by the CFSR reanalysis and locally observed on the ship.

https://doi.org/10.5194/acp-2020-1007
Preprint. Discussion started: 28 October 2020

Atmospheric Chemistry and Physics Discussions

Excluding samples with big errors in meteorological parameters, we obtain the algorithm error of about 5-10 W m^{-2}, which is within the accuracy of the eddy-covariance method during ship measurements.

The differences between the experiments (long-term calculations for the period 1979-2017) with different parameterizations of the roughness length are small and are on average 1-3% of the flux magnitude. In some cases, differences can reach 100-200 W m^{-2}. Parameterizations of Taylor and Yelland (2001) and Oost et al. (2002), which represent the dependence of the roughness length on wave steepness and wave length, respectively, on average overestimate the magnitude of the fluxes, and the parameterization of Drennan et al. (2003) (the dependence of the roughness length on wave height and wave age) steadily underestimates the magnitude of the fluxes over the entire sea compared to the Charnock parameterization. Thus, the effect of explicit accounting for wave parameters is, on average, small and multidirectional, depending on the used parameterization. The modified Charnock formula quite successfully describes the real behavior of the surface roughness even without explicitly taking into account the waves parameters. This can be explained, firstly, by the Charnock parameter dependence on various ranges of wind speed obtained from empirical data, and secondly, by the high correlation between wave parameters and wind speed usually observed. In the climatic aspect, it can be argued that explicit accounting for sea waves in the calculations of heat fluxes can be neglected.

However, in some situations, the choice of a particular roughness parameterization may be important. During storms and cold-air outbreaks, differences between parameterizations increases along with the turbulent heat transfer increase. In some extreme cases, during storms and cold-air outbreaks, the difference T1-C55 reaches 100 W m^{-2}, the difference O2-C55 reaches 700 W m^{-2}.

The difference between the experiments with parameterization D3 and C55 is almost the same in all cases and always decreases (modulo) from west to east of the sea, actually resembling the mean distribution of wave height. Experiments with parameterizations T1 and O2 deviate most strongly from the Charnok parametrization in those areas and at those times when the absolute values of the fluxes are large. The greatest absolute difference between the fluxes is obtained for the simultaneous action of storms and cold-air outbreaks in the northwest and northeast of the sea, i.e. when the values of the fluxes are the greatest. The relative flux difference (the difference normalized to the value of the flux) over the entire sea is greatest during storms (in some areas more than 5%) (Figure 20), but in some areas (in the north, near the ice edge), the relative difference is higher at the simultaneous action of cold-air outbreaks and storms. In all situations, the relative difference is large in the region of the Pechora Sea due to the low absolute values of the fluxes. An area of low absolute and relative values of the flux difference is located to the north-east from Bear Island.

https://doi.org/10.5194/acp-2020-1007
Preprint. Discussion started: 28 October 2020

Atmospheric Chemistry and Physics Discussions

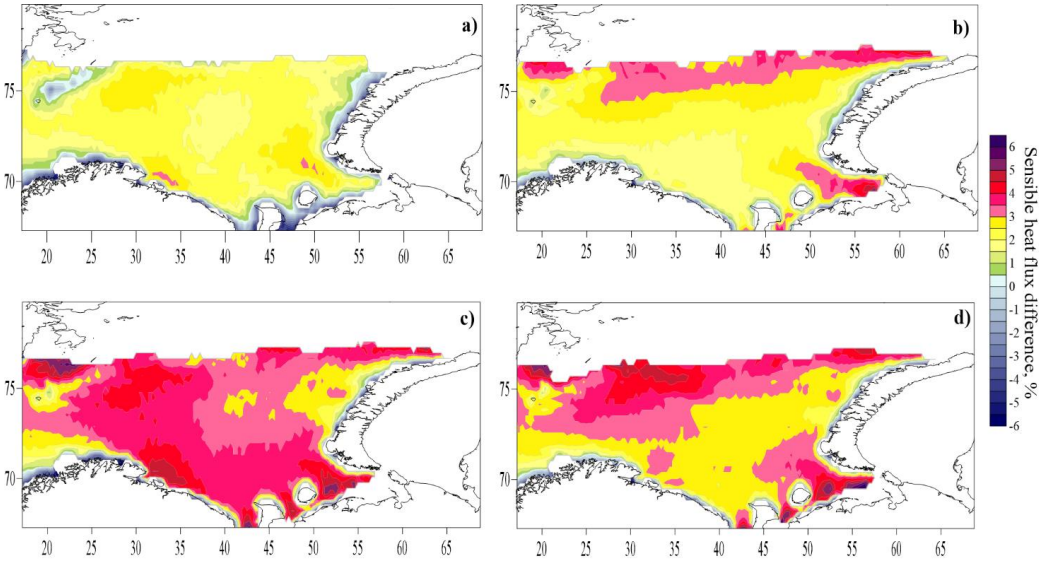

Figure 20. Mean relative difference in sensible heat flux (%) in the experiments T1 - C55 for all cases (a), during cold-air outbreaks (b), during storms (c) and during simultaneously observed storm waves and cold-air outbreaks (d).

Finally, based on the results of our study we can recommend the use of the parametrizations that take into account the wave parameters explicitly in the case of storms, cold-air outbreaks, and especially in the case of simultaneous action of storms and cold-air outbreaks, especially in the northern half of the sea, near the ice edge, in the Pechora Sea and near the coast of the Kola Peninsula (in case of storms).

Data availability

Data and results in this article resulting from numerical simulations are available upon request from the corresponding author.

Author contributions

The concept of the study was jointly developed by SM. SM did the numerical simulations, analysis, visualization and manuscript writing. ASh did the Coare simulations and its visualization. DCh did the calculations of cold-air outbreaks repeatability.

Competing interests.

The authors declare that they have no conflict of interest.

Acknowledgments.

Data analysis funded by the RFBR (project 18-05-60083 Shestakova A.A. and Chechin D.G.). The wave modeling was done with the financial support of the RFBR (project 20-35-70039 Myslenkov S.A.). Authors gratefully thank I.A. Repina for the provided shipborne observations collected during NABOS expeditions.

References

Andreas, E. L.: Thermal and size evolution of sea spray droplets (No. CRREL-89-11). Cold Regions Research and Engineering Lab Hanover NH, 1989.

Arthun, M., Schrum, C.: Ocean surface heat flux variability in the Barents Sea. Journal of Marine Systems, 83(1-2), 88-98, https://doi.org/10.1016/j.jmarsys.2010.07.003, 2010.

https://doi.org/10.5194/acp-2020-1007
Preprint. Discussion started: 28 October 2020

Atmospheric Chemistry and Physics Discussions

Beljaars, A. C. M., & Holtslag, A. A. M.: Flux parameterization over land surfaces for atmospheric models. Journal of Applied Meteorology, 30(3), 327-341, https://doi.org/10.1175/1520-0450(1991)030%3C0327:FPOLSF%3E2.0.CO;2, 1991.

Brodeau, L., Barnier, B., Gulev, S. K., & Woods, C.: Climatologically significant effects of some approximations in the bulk parameterizations of turbulent air–sea fluxes. Journal of Physical Oceanography, 47(1), 5-28, https://doi.org/10.1175/JPO-D-16-0169.1, 2017.

Brümmer, B.: Boundary-layer modification in wintertime cold-air outbreaks from the Arctic sea ice. Bound.-Layer Meteor. 80, 109–125, 1996.

Brunke, M. A., Wang, Z., Zeng, X., Bosilovich, M., & Shie, C. L.: An assessment of the uncertainties in ocean surface turbulent fluxes in 11 reanalysis, satellite-derived, and combined global datasets. Journal of Climate, 24(21), 5469-5493, https://doi.org/10.1175/2011JCLI4223.1, 2011.

Brutsaert, W.: Evaporation into the Atmosphere—Theory, History, and Applications. D. Reidel, 299 pp, 1982.

Chechin D.G, Lüpkes C., Repina I.A., Gryanik V.M.: Idealized dry quasi-2D mesoscale simulations of cold-air outbreaks over the marginal sea-ice zone with fine and coarse resolution. J. Geophys. Res., 118, pp. 8787-8813, doi: 10.1002/jgrd.50679, 2013.

Chechin D.G., Zabolotskikh E.V., Repina I.A., Shapron B.: Influence of baroclinicity in the atmospheric boundary layer and Ekman friction on the surface wind speed during cold-air outbreaks in the Arctic, Izv. Atmos. Ocean. Phys., Vol. 51 No. 2, pp. 127–137, doi: 10.1134/S0001433815020048, 2015.

Chechin D.G, Lüpkes C.: Boundary-layer development and low-level baroclinicity during high-latitude cold-air outbreaks: a simple model. Boundary-Layer Meteorol 162: 91. https://doi.org/10.1007/s10546-016-0193-2, 2017.

Chechin, D. G. and Lüpkes, C.: Baroclinic low-level jets in Arctic marine cold-air outbreaks. IOP Conference Series: Earth and Environmental Science, IOP Publishing, 231, 012011, 2019.

Charles, E., Hemer, M.: Parameterization of a wave-dependent surface roughness: A step towards a fully coupled atmosphere-ocean-sea ice-wave system. In 13th International Workshop on Wave Hindcasting and Forecasting and 4th Coastal Hazard Symposium, 2013.

Charnock, H.: Wind stress on a water surface. Quarterly Journal of the Royal Meteorological Society, 81(350), 639-640, 1955.

Drennan, W. M., Graber, H. C., Hauser, D. and Quentin, C.: On the wave age dependence of wind stress over pure wind seas. Journal of Geophysical Research, 108(C3), 8062, 2003.

ECMWF: Part VII: ECMWF wave model. IFS Documentation Cy31r1, 56 pp. [Available online at http://www.ecmwf.int/research/ifsdocs/CY31r1/WAVES/IFSPart7.pdf.], 2007.

Fairall, C. W., Bradley, E. F., Hare, J. E., Grachev, A. A., & Edson, J. B.: Bulk parameterization of air–sea fluxes: Updates and verification for the COARE algorithm. Journal of climate, 16(4), 571-591, https://doi.org/10.1175/1520-0442(2003)016%3C0571:BPOASF%3E2.0.CO;2, 2003.

Fairall, C. W., Bradley, E. F., Rogers, D. P., Edson, J. B., & Young, G. S.: Bulk parameterization of air-sea fluxes for tropical ocean-global atmosphere coupled-ocean atmosphere response experiment. Journal of Geophysical Research: Oceans, 101(C2), 3747-3764, https://doi.org/10.1029/95JC03205, 1996.

Fletcher, J., S. Mason, and C. Jakob: The Climatology, Meteorology, and Boundary Layer Structure of Marine Cold Air Outbreaks in Both Hemispheres. J. Climate, **29**, 1999–2014, https://doi.org/10.1175/JCLI-D-15-0268.1, https://doi.org/10.1175/JCLI-D-15-0268.1, 2016.

Grachev, A.A., Fairall, C.W. & Bradley, E.F.: Convective Profile Constants Revisited. Boundary-Layer Meteorology 94(3): 495-515, 2000.

Grønas A., Skeie P.: A case study of strong winds at an Arctic front. Tellus 51:865–879, https://doi.org/10.3402/tellusa.v51i5.14498, 1999.

Häkkinen, S., Cavalieri, D. J.: A study of oceanic surface heat fluxes in the Greenland, Norwegian, and Barents Seas. Journal of Geophysical Research: Oceans, 94(C5), 6145-6157, https://doi.org/10.1029/JC094iC05p06145, 1989.

Ivanov, V., Varentsov, M., Matveeva, T., Repina, I., Artamonov, A., & Khavina, E.: Arctic Sea Ice Decline in the 2010s: The Increasing Role of the Ocean—Air Heat Exchange in the Late Summer. Atmosphere, 10(4), 184, 2019.

Ivanov V. V., Timokhov L.A.: Atlantic water in the arctic circulation transpolar system. Russian Meteorology and Hydrology. Vol. 44, no. 4. 238–249, https://doi.org/10.3103/S1068373919040034, 2019.

Janssen, P. A.: Quasi-linear theory of wind-wave generation applied to wave forecasting. Journal of physical oceanography, 21(11), pp. 1631-1642, https://doi.org/10.1175/1520-0485(1991)021%3C1631:QLTOWW%3E2.0.CO;2, 1991.

Jones, I. S., Toba, Y. (Eds.).:Wind stress over the ocean. Cambridge University Press, 2001.

Kaimal, J. C., Wyngaard, J. C., Izumi, Y., and Cote 0. R.: Spectral Characteristics of Surface-Layer Turbulence. Quart. J. Roy. Meteorol. Soc. 98, 563-589, 1972.

Kim, T., Moon, J. H., Kang, K.: Uncertainty and sensitivity of wave-induced sea surface roughness parameterisations for a coupled numerical weather prediction model. Tellus A: Dynamic Meteorology and Oceanography, 70(1), 1-18, https://doi.org/10.1080/16000870.2018.1521242, 2018.

Kolstad E. W., Bracegirdle T.J.: Marine cold-air outbreaks in the future: an assessment of IPCC AR4 model results for the Northern Hemisphere. Clim. Dyn. 30:871–885. doi:10.1007/s00382-007-0331-0, https://doi.org/10.1007/s00382-007-0331-0, 2008.

Kolstad, E.W., Bracegirdle, T.J. and Seierstad, I.A.: Marine cold-air outbreaks in the North Atlantic: temporal

https://doi.org/10.5194/acp-2020-1007
Preprint. Discussion started: 28 October 2020

Atmospheric Chemistry and Physics Discussions

distribution and associations with large-scale atmospheric circulation. Clim Dyn **33,** 187–197, doi:10.1007/s00382-008-0431-5, 2009.

Kolstad E.W.: Extreme small-scale wind episodes over the Barents Sea: When, where and why? Clim Dyn, 45, 2137-2150, doi:10.1007/s00382-014-2462-4, 2015.

Large W. G. and S. G. Yeager: The global climatology of an interannually varying air-sea flux data set. Climate Dynamics, **33**, 341-364 (DOI: 10.1007/s00382-008-0441-3), 2009.

Liu, W. T., Katsaros, K. B., & Businger, J. A.: Bulk parameterization of air-sea exchanges of heat and water vapor including the molecular constraints at the interface. Journal of the Atmospheric Sciences, 36(9), 1722-1735, 1979.

Liu Q., Babanin A.,Zieger S., Young I., Guan C.: Wind and wave climate in the Arctic Ocean as observed by altimeters. J. Climate. 2016. V. 29(22). P. 7957–7975, https://doi.org/10.1175/JCLI-D-16-0219.1, 2016.

Mahrt, L., Vickers, D., Frederickson, P., Davidson, K., & Smedman, A. S.: Sea-surface aerodynamic roughness. Journal of Geophysical Research: Oceans, 108(C6), https://doi.org/10.1029/2002JC001383, 2003.

Moore G.W.K.: The Novaya Zemlya Bora and its impact on Barents Sea air-sea interaction, Geophys. Res. Lett., 40, 3462 — 3467, doi:10.1002/grl.50641, 2013.

Myslenkov S., Medvedeva A., Arkhipkin V., Markina M., Surkova G., Krylov A., Dobrolyubov S., Zilitinkevich S., Koltermann P.: Long-term statistics of storms in the Baltic, Barents and White Seas and their future climate projections. Geography, Environment, Sustainability.V. 11. № 1. P. 93–112, https://doi.org/10.24057/2071-9388-2018-11-1-93-112, 2018.

Myslenkov S.A., Arkhipkin V.S., Koltermann K.P.: Evaluation of swell height in the Barents and White Seas, Moscow University Bulletin, Series 5. Geography. №5, pp.59-66, 2015.

Myslenkov, S.A., Markina, M.Yu., Arkhipkin, V.S., Tilinina, N.D.: Frequency of storms in the Barents sea under modern climate conditions. Vestnik Moskovskogo Universiteta, Seriya 5: Geografiya. Volume, Issue 2, 2019, Pages 45-54, 2019.

Myslenkov S.A., Markina M. Yu., Kiseleva S.V. et al.: Estimation of Available Wave Energy in the Barents Sea. Thermal Engineering. 65, 7, 411–419, https://doi.org/10.1134/S0040601518070054, 2018.

Oost, W. A., Komen, G. J., Jacobs, C. M. J., & Van Oort, C.: New evidence for a relation between wind stress and wave age from measurements during ASGAMAGE. Boundary-Layer Meteorology, 103(3), 409-438, 2002.

Pan, Y., Sha, W., Zhu, S., Ge, S.: A new parameterization scheme for sea surface aerodynamic roughness. Progress in Natural Science, 18(11), 1365-1373, https://doi.org/10.1023/A:1014913624535, 2008.

Papritz, L. and T. Spengler: A Lagrangian Climatology of Wintertime Cold Air Outbreaks in the Irminger and Nordic Seas and Their Role in Shaping Air–Sea Heat Fluxes. J. Climate, **30**, 2717–2737, https://doi.org/10.1175/JCLI-D-16-0605.1, 2017.

Pithan, F. , Svensson, G. , Caballero, R. , Chechin, D. , Cronin, T. W. , Ekman, A. M. L. , Neggers, R. , Shupe, M. D. , Solomon, A. , Tjernström, M. and Wendisch, M.: Role of air-mass transformations in exchange between the Arctic and mid-latitudes , Nature Geoscience, 11 (11), pp. 805-812, https://doi.org/10.1038/s41561-018-0234-1, 2018.

Prakash, K. R., Pant, V., Nigam, T.: Effects of the Sea Surface Roughness and Sea Spray-Induced Flux Parameterization on the Simulations of a Tropical Cyclone. Journal of Geophysical Research: Atmospheres, 124(24), https://doi.org/10.1029/2018JD029760, 2019.

Rahmstorf, S., Ganopolski, A.: Long-Term Global Warming Scenarios Computed with an Efficient Coupled Climate Model. Climatic Change 43, 353–367. https://doi.org/10.1023/A:1005474526406, 1999.

Renfrew, I. A., Moore, G. K., Guest, P. S., & Bumke, K.: A comparison of surface layer and surface turbulent flux observations over the Labrador Sea with ECMWF analyses and NCEP reanalyses. Journal of Physical Oceanography, 32(2), 383-400, https://doi.org/10.1175/1520-0485(2002)032%3C0383:ACOSLA%3E2.0.CO;2, 2002.

Saha S. et al.: The NCEP climate forecast system reanalysis. Bul. of the American Meteorological Society. V. 91. № 8. P. 1015–1057, https://doi.org/10.1175/2010BAMS3001.1, 2010.

Saha S. et al.:The NCEP Climate Forecast System Version 2. J. Climate. 27, 2185—2208, https://doi.org/10.1175/JCLI-D-12-00823.1, 2014.

Savijärvi H. I.: Cold air outbreaks over high-latitude sea gulfs, Tellus A: Dynamic Meteorology and Oceanography, 64:1, DOI: 10.3402/tellusa.v64i0.12244, 2012.

Semedo A, Sušelj K, Rutgersson A, Sterl A.: A global view on the wind sea and swell climate and variability from ERA-40. J Clim 24(5):1461–1479, https://doi.org/10.1175/2010JCLI3718.1, 2011.

Shimura, T., Mori, N., Takemi, T., Mizuta, R.: Long-term impacts of ocean wave-dependent roughness on global climate systems. Journal of Geophysical Research: Oceans, 122(3), 1995-2011, https://doi.org/10.1002/2016JC012621, 2017.

Simonsen, K., Haugan, P. M.: Heat budgets of the Arctic Mediterranean and sea surface heat flux parameterizations for the Nordic Seas. Journal of Geophysical Research: Oceans, 101(C3), 6553-6576, https://doi.org/10.1029/95JC03305, 1996.

Skeie P.: Meridional flow variability over the Nordic Seas in the Arctic Oscillation framework. Geophys. Res. Lett. 27:2569-2572. https://doi.org/10.1029/2000GL011529, 2000.

Smedsrud, L. H., et al.:The role of the Barents Sea in the Arctic climate system, Rev. Geophys., 51, 415–449, doi:10.1002/rog.20017, 2013.

https://doi.org/10.5194/acp-2020-1007
Preprint. Discussion started: 28 October 2020

Atmospheric Chemistry and Physics Discussions

734 Smith, S. D.: Coefficients for sea surface wind stress, heat flux, and wind profiles as a function of wind speed
735 and temperature. Journal of Geophysical Research: Oceans, 93(C12), 15467-15472, 1988.
736 Stopa J., Ardhuin F.,Girard-Ardhuin F.: Wave climate in the Arctic 1992-2014: seasonality and trends.
737 Cryosphere, 10(4), pp.1605-1629, https://doi.org/10.5194/tc-10-1605-2016, 2016.
738 Taylor, P. K., & Yelland, M. J.: The dependence of sea surface roughness on the height and steepness of the
739 waves. Journal of physical oceanography, 31(2), 572-590, https://doi.org/10.1175/1520-
740 0485(2001)031%3C0572:TDOSSR%3E2.0.CO;2, 2001.
741 Tolman, H.: The WAVEWATCH III Development Group User Manual and System Documentation of
742 WAVEWATCH III version 4.18. Tech. Note 316, NOAA/NWS/NCEP/MMAB, 2014, available at:
743 http://polar.ncep.noaa.gov/waves/wavewatch/ manual.v4.18.pdf (last access: 23 June 2018), 2014.
744 Varentsov, M.I., Repina, I.A., Artamonov, A. Yu., Khavina, E.M., & Matveeva, T.A.: Experimental studies
745 of energy transfer and the dynamics of the atmospheric boundary layer in the Arctic in the summer. Proceedings of
746 the Hydrometeorological Research Center of the Russian Federation, (361), 95-127, 2016.
747 Wheeler, D. D., Harvey, V. L., Atkinson, D. E., Collins, R. L., and Mills, M. J.: A climatology of cold air
748 outbreaks over North America: WACCM and ERA-40 comparison and analysis, J. Geophys. Res., 116, D12107,
749 doi:10.1029/2011JD015711, 2011.
750 Wind and Wave Climate Handbook. Barents, Okhotsk, and Caspian Seas: Ed. by L. I. Lopatukhin, et al.
751 (Russian Maritime. Register Shipping., St. Petersburg, 2003), 2003.
752 Wu, B., J. Wang, and J.E. Walsh: Dipole Anomaly in the Winter Arctic Atmosphere and Its Association with
753 Sea Ice Motion. J. Climate, 19, 210–225, https://doi.org/10.1175/JCLI3619.1, 2006.
754 Yu, L., & Jin, X.: Satellite-based global ocean vector wind analysis by the Objectively Analyzed Air-sea
755 Fluxes (OAFlux) Project: Establishing consistent vector wind time series from July 1987 onward through synergizing
756 microwave radiometers and scatterometers (Vol. 1). WHOI OAFlux Tech. Rep. WHOI-OA-2011, 2011.
757 Zilitinkevich S.S., Grachev A.A., Fairall C.W.: Scaling reasoning and field data on the sea surface roughness
758 lengths for scalars. J. Atmos. Sci. V. 58. P. 320–325, 2001.